

Lossless plasmons in highly mismatched alloys

Hassan Allami¹ and Jacob J. Krich^{1, a)}

Department of Physics, University of Ottawa, Ottawa, ON K1N 6N5, Canada

We explore the potential of highly mismatched alloys (HMAs) for realizing lossless plasmonics. Systems with a plasmon frequency at which there are no interband or intraband processes possible are called lossless, as there is no 2-particle loss channel for the plasmon. We find that the band splitting in HMAs with a conduction band anticrossing guarantees a lossless frequency window. When such a material is doped, producing plasmonic behavior, we study the conditions required for the plasmon frequency to fall in the lossless window, realizing lossless plasmons. Considering a generic class of HMAs with a conduction band anticrossing, we find universal contours in their parameter space within which lossless plasmons are possible for some doping range. Our analysis shows that HMAs with heavier effective masses are most promising for realizing a lossless plasmonic material.

The field of plasmonics relies on surface plasmon polariton (SPP) modes, which can be excited on metal-dielectric interfaces.^{1,2} These SPP modes can enhance and concentrate electric fields at subwavelength scale,^{3–5} with applications in metamaterials,⁶ optoelectronics,^{7–12} and photocatalysis.¹³ The applications range from the established surface-enhanced Raman scattering (SERS) technique¹⁴ to new proposals in quantum optics¹⁵ such as quantum teleportation.¹⁶

In practice, many plasmonic applications are hindered by loss and decay of the plasmonic modes.^{17–19} Although some plasmonic applications such as SERS are still viable in the presence of losses,²⁰ and in cases such as photodetection and photocatalysis losses are beneficial,^{12,13,17,21} the loss problem is one of the main challenges in the field of plasmonics and metamaterials.^{6,22}

Many approaches have been proposed to reduce and mitigate losses in plasmonic systems, including improvements in fabrication,²³ employing optical gain,²⁴ spectrum modification,²⁵ and of course, searching for alternative plasmonic materials.^{26–31} Khurgin and Sun presented a strategy to find lossless plasmonic modes by considering the fundamental conditions creating loss.³² Often the most important loss channel for SPPs is decay into electron-hole excitation. They argue that dissipating the energy of an electromagnetic mode in this way requires empty electronic states. In a material with the appropriate electronic structure, such empty states may be absent for a range of energies, offering a lossless window of frequencies. Hence they conclude that if the plasma frequency falls inside the lossless window, the primary decay mechanism will have been removed, producing an essentially lossless plasmonic material. Khurgin and Sun proposed a few classes of materials that can potentially realize their conditions for lossless plasmons, and some of them have been investigated with promising results.^{33–35}

In this work, we propose highly mismatched alloys (HMA) as a candidate class for realizing mid- to far-IR lossless plasmons. This possibility was briefly mentioned but not elaborated in Ref. 36. We consider the

one-particle and plasmonic structure of HMAs and find the alloying and doping requirements to achieve lossless plasmons. We describe universal contours in the parameter space of HMAs in which lossless plasmons are possible for some range of doping. We show the alloy fractions and plasmon frequencies that occur in the lossless window for the ZnCdTeO system and suggest that HMAs with large effective masses are most likely to be able to realize the conditions needed for lossless plasmons. In the remainder of this work, we use the term “lossless window” in the sense of Ref. 32.

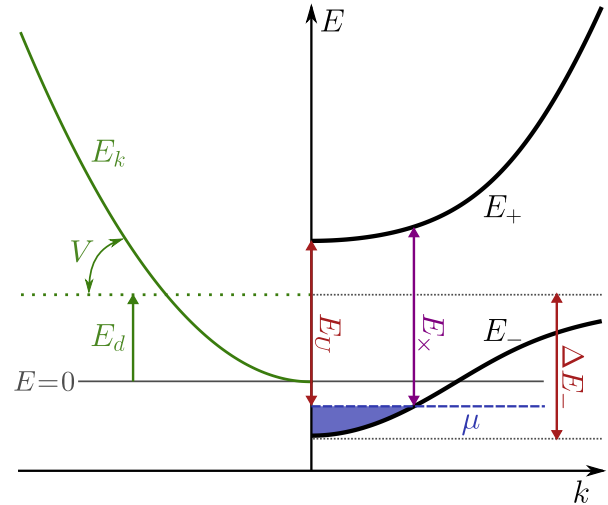


FIG. 1. (left) The conduction band of the host material E_k , and the localized state E_d , coupled through V . The energy reference is at the bottom of E_k . (right) The split bands of BAC model, E_+ and E_- . The interband loss starts for energies larger than E_U , and for the energies below E_- bandwidth ΔE_- , intraband dissipation is possible. Doping determines the chemical potential μ . The interband transitions bound plasmon energy $\hbar\omega_p$ to $E_x = \min_{k < k_F} (E_k^+ - E_k^-)$.

HMAs are a class of semiconductor alloys where the alloying elements have very different electronegativity than that of the host. Shan et al. described that localized states form around the mismatching elements and pro-

^{a)}School of Electrical Engineering and Computer Science, University of Ottawa, Ottawa, ON K1N 6N5, Canada

posed a band anticrossing (BAC) model, which successfully describes the energy spectrum of HMAs.³⁷ According to the BAC model, the localized level E_d and the host conduction band (CB) with dispersion $E_{\mathbf{k}}$ hybridize at each wavevector \mathbf{k} independently with a single coupling factor V (see Fig. 1). Two split bands emerge, with dispersion

$$E_{\pm} = \frac{1}{2} \left(E_k + E_d \pm \sqrt{(E_k - E_d)^2 + 4V^2x} \right), \quad (1)$$

where x is the alloy fraction of the mismatching element. The two split bands E_{\pm} are shown as solid black curves in Fig. 1. Here we consider a class of HMAs where the localized level anticrosses with a parabolic CB with $E_{\mathbf{k}} = \hbar^2 k^2/2m$, the bottom of which is taken to be the zero energy level, as shown in Fig. 1. All such HMAs are described by three scalar parameters: $V\sqrt{x}$, E_d , and m .

We now describe the range of excitation energies that can be lost to particle-hole excitations in a doped HMA. We consider that the excess electrons occupy the E_- band, and we consider zero temperature, so the chemical potential μ lies somewhere in E_- , as in Fig. 1. The free electrons in E_- produce plasmonic behavior³⁸ while at the same time providing two channels for dissipating energy. First, an excitation of any amount of energy up to the bandwidth ΔE_- of the E_- band can move an electron from a filled state to an empty state within the E_- band. The excited electron and hole can then dissipate their energy into a set of excitations with infinitesimal energy by moving electrons near the Fermi surface to nearby empty states. Figure 2 shows the range of excitation energies and μ where dissipation into particle-hole excitations can occur; the grey area under the horizontal dashed red line represents this intraband lossy region. Second, an electron can be excited to the E_+ band. The minimum energy for such interband transitions is $E_U \equiv E_+(k=0) - \mu$, which is labeled in Figs. 1 and 2. Excitations with energy higher than E_U can then be lost through a combination of inter- and intra-band transitions. The grey area above the slanted dashed line in Fig. 2 represents this second lossy region.

Excitations with energy between ΔE_- and E_U are lossless, i.e., have no single-particle decay channels, if $E_U > \Delta E_-$. The white area in Fig. 2 shows this lossless window, which linearly shrinks with increasing μ . Measuring energies from the bottom of $E_{\mathbf{k}}$, it turns out that $E_+(k=0) = \Delta E_-$, so $E_U = \Delta E_- - \mu$. So there is always a lossless window if $\mu < 0$. Moreover, since the minimum of E_- is always negative, for any HMA there is always a doping level below which there exists a lossless window.

The next step is to check when the plasmon energy $\hbar\omega_p$ falls in the lossless window. $\hbar\omega_p$ depends on the carrier concentration and hence on μ , which ranges between the bottom and the top of E_- at zero temperature. As shown by the blue curve in Fig. 2, $\hbar\omega_p$ initially rises with μ as free carriers enter the E_- band and falls back to zero when the band is full.³⁸ Depending on the HMA param-

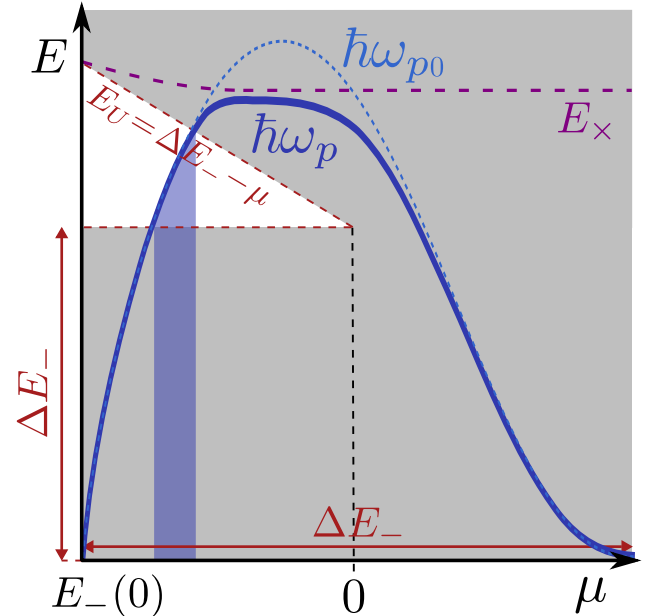


FIG. 2. The lossless window of excitation energies (white area) and $\hbar\omega_p$ (dark blue line) as a function of chemical potential μ . $\hbar\omega_p$ is bounded by $\hbar\omega_{p0}$ and E_x . The blue shaded strip shows the range of μ where $\hbar\omega_p$ falls in the lossless window.

eters, $\hbar\omega_p$ can fall in the lossless window for some range of doping, as in the case in the figure.

In previous work,³⁸ we found that ω_p for this class of HMAs obeys

$$\omega_p^2 = \omega_{p0}^2 \left[1 + \left(\frac{mc\ell}{\hbar} \right)^2 I_{\times}(\omega_p) \right]^{-1}, \quad (2)$$

in which ω_{p0} is the plasma frequency in the absence of interband transitions, and the second term in the bracket represents the effect of interband transitions, where ℓ is a length scale that determines the strength of the transitions, which needs to be determined for each HMA. We provide more details in Section A of the supplementary material. Ref. 38 derived a closed algebraic form for ω_{p0} and an integral for $I_{\times}(\omega)$, which is always positive and diverges as $\hbar\omega$ approaches $E_x \equiv \min_{k < k_F} (E_{\mathbf{k}}^+ - E_{\mathbf{k}}^-)$, where k_F is the Fermi momentum. Therefore, $\hbar\omega_p$ is bounded by $\hbar\omega_{p0}$ and E_x , as Fig. 2 shows. Note that since E_x is the minimum distance between E_+ and the filled part of E_- at the same \mathbf{k} , it is always larger than E_U , which does not have the same \mathbf{k} restriction (see Figs. 1 and 2).

If we normalize all energies to $2mc^2$, then we can accommodate this entire class of HMAs in a 2D plane spanned by $V\sqrt{x}/2mc^2$ and $E_d/2mc^2$. But since $2mc^2$ for typical semiconductors is of the order of MeV, while meV is a more relevant unit for typical $V\sqrt{x}$ and E_d , we normalize energies using $E_m \equiv 2mc^2 \times 10^{-9}$ and define $\tilde{V} \equiv V/E_m$, $\tilde{E}_d \equiv E_d/E_m$. For the bare electron mass

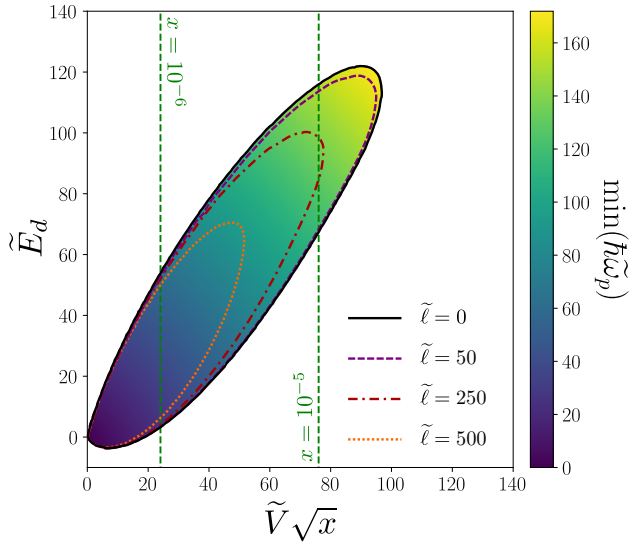


FIG. 3. Universal contours showing regions with lossless plasmons for several $\tilde{\ell} \equiv mcl/\hbar$, with energies all normalized by $E_m \equiv 2mc^2 \times 10^{-9}$. The color scale shows the smallest normalized plasmon energy in the lossless window, which is always equal to $\Delta E_- / E_m$, independent of $\tilde{\ell}$. The green almost-vertical dashed lines show the locus of $\text{Zn}_{1-y}\text{Cd}_y\text{Te}_{1-x}\text{O}_x$, for $x = 10^{-6}$ and $x = 10^{-5}$, as y changes approximately between 0.27 and 0.29.

$m_e, E_m \approx 1$ meV, so for any other effective mass m one can scale all dimensionless energies by m/m_e to find the approximate value in meV.

We can determine for any point in the $(\tilde{V}\sqrt{x}, \tilde{E}_d)$ plane whether there is a doping range in which $\hbar\omega_p$ falls in the lossless window, realizing lossless plasmons. Then, with fixed $\ell \equiv lmc/\hbar$, where \hbar/mc is the reduced Compton wavelength, there is a universal contour in the $(\tilde{V}\sqrt{x}, \tilde{E}_d)$ plane within which such HMAs fall. Fig. 3 shows these universal contours of lossless plasmonic HMAs for a few values of $\tilde{\ell}$. The solid black contour shows the $\ell = 0$ case without interband transitions, where $\omega_p = \omega_{p0}$. The contours do not vary significantly from the $\tilde{\ell} = 0$ case until $\tilde{\ell} \gtrsim 100$ since $I_x(\omega)$ in Eq. (2) is significant only for $\hbar\omega_p$ near E_x . But since in the lossless window $\hbar\omega_p < E_U < E_x$, the interband processes can move $\hbar\omega_p$ away from $\hbar\omega_{p0}$ only when $\tilde{\ell}$ is large. For estimated typical values of $\ell = 1 - 10 \text{ \AA}$, $\tilde{\ell} \approx (250 - 2500)m/m_e$. Using ω_{p0} in place of ω_p , as in the $\tilde{\ell} = 0$ case, allows us to derive an analytic expression for the lossless contour, which is presented in Section B of the supplementary material.

The color scale of Fig. 3 shows the smallest $\hbar\omega_p$ in the lossless window. As Fig. 2 shows, the minimum value of $\hbar\omega_p$ in the lossless window is always ΔE_- , which does not depend on ℓ . Therefore, $\min(\hbar\omega_p/E_m)$ is the same for lossless contours belonging to different $\tilde{\ell}$. Although the largest $\hbar\omega_p$ in the lossless window is somewhat different

TABLE I. The range of BAC parameters for $\text{Zn}_{1-y}\text{Cd}_y\text{Te}_{1-x}\text{O}_x$.^{39,40}

Parameters	$y = 0$	$y = 1$
E_d [eV]	-0.27	0.38
V [eV]	2.8	2.2
m [m_e]	0.117	0.09

for each $\tilde{\ell}$, the typical difference between $\max(\hbar\omega_p)$ and $\min(\hbar\omega_p)$ is of the order of a few E_m for all cases.

Since $E_m \propto m$, Fig. 3 shows that HMAs with heavier m can achieve lossless plasmons for a wider range of $V\sqrt{x}$ and E_d . Since the typical values of V are on the order of eV, increasing the range of $V\sqrt{x}$ is particularly crucial because otherwise the required x may be too small to realistically show alloying effects.

To illustrate this point, consider the quaternary HMA, $\text{Zn}_{1-y}\text{Cd}_y\text{Te}_{1-x}\text{O}_x$, in which oxygen is the mismatching element in ZnCdTe . Table I shows the range of BAC parameters for this quaternary, determined from studies of alloy-dependent band gap.^{39,40} Doping of the E_- band with chlorine has been demonstrated,⁴¹ and this system can realize different values of E_d by tuning the cadmium content y . The E_d range covered in Fig. 3 corresponds to y between 0.27 and 0.29. The two nearly vertical dashed green lines in Fig. 3 show the locus of ZnCdTeO in the HMA parameter space, as y varies for two fixed values of oxygen fraction, $x = 10^{-6}$ and $x = 10^{-5}$, with details of the assumed bowing parameters described in Section C of the supplementary material. This range of y , which produces E_d near zero, allows overlap of ω_p with the lossless region when x is sufficiently small. As the smallest x for which the BAC model applies is unexplored, it is not clear whether these particular parameter ranges are experimentally realizable. ZnCdTe has $m \approx 0.1m_e$, so in the lossless window we find $\hbar\omega_p$ from 3 to 6 meV for $x = 10^{-6}$ and 13 to 16 meV for $x = 10^{-5}$. For these small $\hbar\omega_p$, phonons could directly couple to the plasmons, providing a new channel for dissipation and breaking the lossless condition. A material with a heavier effective mass would allow both for larger x and lossless plasmons with higher $\hbar\omega_p$.

Observing these low plasma frequencies may require low temperatures, as Eq. (2) is derived at $T = 0$. At higher temperatures, the occupation fraction of states in the E_- band must be taken into account. Nonetheless, the suppression of electronic decay channels in this lossless window should still be visible in experiments.

Although overall HMAs with heavier m are more promising in realizing lossless plasmons, not everything favors them. Interband transitions shrink the lossless contour, as shown in Fig. 3, and $\tilde{\ell}$ increases linearly with m . Lighter m can allow smaller $\tilde{\ell}$ and a larger lossless contour.

The two most explored classes of conduction band HMAs are III-V nitrides and II-VI oxides.⁴² Given the

low effective masses of the conduction bands in these materials, the lossless plasmonic window will occur for THz-frequency ω_p with extremely light alloying. As new HMAs with larger effective masses in their host bands are found, they will provide further opportunities to realize lossless plasmonic materials. HMAs with valence band anticrossings^{43,44} could be good candidates, as they typically have heavier effective masses, though the theory of their plasmon frequencies has not yet been worked out. HMAs present exciting potential for realizing a lossless plasmonic medium and are worth more theoretical and experimental investigations.

See the supplementary material for the details of the plasma frequency equation, the analytic expression of the lossless contour for the case of $\ell = 0$, and the locus of ZnCdTeO in the HMA parameter space.

We acknowledge funding from the NSERC CREATE TOP-SET program, Award Number 497981.

AUTHOR DECLARATIONS

Conflict of Interest

The authors have no conflicts to disclose.

DATA AVAILABILITY

The data that support the findings of this study are openly available at <https://github.com/hassan-allami/Lossless-HMAs>.⁴⁵

Appendix A: Deriving Eq. (2) for the plasma frequency

Eq. (2) of the main text is the rewriting of Eq. (20) of Ref. 38. In Ref. 38, ω_{p0} is defined in Eq. (18) in terms of $E_{k_F} = \hbar^2 k_F^2 / 2m$. By solving $E_-|_{k=k_F} = \mu$ for E_{k_F} , one can find $E_{k_F} = \mu + V^2 x / (E_d - \mu)$. This form allows rewriting Eq. (18) of Ref. 38 to give $\hbar\omega_{p0}(\mu)$ as

$$\hbar\omega_{p0} = \sqrt{\frac{8\alpha}{3\pi}} (2mc^2)^{1/4} \left(\frac{V^2 x}{E_d - \mu} + \mu \right)^{3/4} \left(\frac{(E_d - \mu)^2}{(E_d - \mu)^2 + V^2 x} \right)^{3/2}, \quad (\text{A1})$$

where $\alpha = e^2/\hbar c$ is the fine structure constant.

The dimensionless I_\times can be expressed as

$$I_\times(\tilde{\omega}) = \frac{4\alpha\tilde{V}^2 x}{\pi} \int_0^{\tilde{k}_F} \frac{\tilde{k}^2 d\tilde{k}}{(\tilde{E}_+ - \tilde{E}_-) [(\tilde{E}_+ - \tilde{E}_-)^2 - (\hbar\tilde{\omega})^2]}, \quad (\text{A2})$$

where all energies are in units of $E_m \equiv 2mc^2 \times 10^{-9}$ and all wavevectors are in units of $k_m \equiv mc/\hbar \times 10^{-3}$. This form shows that I_\times is proportional to α , so it is generally small except near where it diverges. It diverges at the smallest ω where $\hbar\omega = \min(E_+ - E_-)$ for some k in the integration domain, which motivates the definition of $E_\times = \min_{k < k_F} (E_+ - E_-)$.

Appendix B: Finding the lossless contour without interband transitions

To find the lossless contour for the case of $\ell = 0$, we need to find the set of HMA parameters for which $\hbar\omega_{p0}$ falls in the lossless window for any μ . As Fig. 2 shows, $\hbar\omega_{p0}(\mu)$ has a maximum. We start by locating this maximum point μ_{\max} . It is more convenient to find the maximum point for $(\hbar\omega_{p0})^4$, which is also μ_{\max} . We define $\lambda = \tilde{E}_d/\tilde{V}\sqrt{x}$ and $\nu = \tilde{\mu}/\tilde{V}\sqrt{x}$. Then using Eq. (A1) to solve $\partial(\hbar\omega_{p0})^4 / \partial\nu = 0$ gives, after dividing out constants,

$$\frac{(\lambda - \nu)^8 (\nu^2 - \lambda\nu - 1)^2 [\nu^4 - 4\lambda\nu^3 + 6(\lambda^2 + 1)\nu^2 - 4(\lambda^3 + 2\lambda)\nu + (\lambda^2 + 3)(\lambda^2 - 1)]}{[(\lambda - \nu)^2 + 1]^7} = 0. \quad (\text{B1})$$

Since the largest μ in the lossless window is $\mu = 0$ (see Fig. 2), we must find whether μ_{\max} is negative.

When $E_d > 0$, note from Eq. (B1) that when $\nu = \mu = 0$, which is the right edge of the lossless window, the sign of Eq. (B1) is determined by the sign of $\lambda - 1$. So $\mu_{\max} \geq 0$ if $\lambda \geq 1$. In this case $\max_{\mu < 0} (\hbar\omega_{p0}) = \hbar\omega_{p0}|_{\mu=0}$. Note that the lossless window is open only for $\mu < 0$ and requires $\hbar\omega_p > \Delta E_-$, so in this case $\hbar\omega_{p0}$ can fall inside the window if

$\hbar\omega_{p0}|_{\mu=0} > \Delta E_-$. Therefore, if $E_d \geq V\sqrt{x}$, the lossless plasmonic region in the HMA parameter space is determined by

$$\sqrt{\frac{8\alpha}{3\pi}} \left(\frac{2mc^2}{E_m} \right)^{1/4} \left(\frac{\tilde{V}^2 x}{\tilde{E}_d} \right)^{3/4} \frac{\tilde{E}_d^3}{(\tilde{E}_d^2 + \tilde{V}^2 x)^{3/2}} > \frac{\tilde{E}_d + \sqrt{\tilde{E}_d^2 + 4\tilde{V}^2 x}}{2}, \quad (\text{B2})$$

where we used Eq. (A1) for $\hbar\omega_{p0}$, and $\Delta E_- = \frac{1}{2}(E_d + \sqrt{E_d^2 + 4V^2 x})$, which can be derived from Eq. (1).

When $E_d < V\sqrt{x}$ and hence $\mu_{\max} < 0$, then the lossless window is open at μ_{\max} , so $\hbar\omega_{p0}$ falls in the lossless window when $\max(\hbar\omega_{p0}) > \Delta E_-$. For $E_d < 0$, we always have $\mu_{\max} < 0$, because μ_{\max} must fall within the E_- band and $E_d < 0$ is the top of the E_- band.

To find μ_{\max} , notice that $(\lambda - \nu)^8(\nu^2 - \lambda\nu - 1)^2$ is zero only when μ is at the bottom or top of the E_- band, where $\omega_{p0} = 0$. Then Eq. B1 says that μ_{\max} is determined by the real roots of $[\nu^4 - 4\lambda\nu^3 + 6(\lambda^2 + 1)\nu^2 - 4(\lambda^3 + 2\lambda)\nu + (\lambda^2 + 3)(\lambda^2 - 1)]$. This term always has two real roots, and only one of them corresponds to a μ inside the E_- band. Picking the relevant root and using $\tilde{\mu} = \nu\tilde{V}\sqrt{x}$, we obtain

$$\begin{aligned} \tilde{\mu}_{\max} &= \tilde{E}_d \left(1 - \sqrt{\frac{\tilde{V}^2 x A}{\tilde{E}_d^2}} \right) - \sqrt{\tilde{V}^2 x B}, \\ A &= \left(1 + \frac{\tilde{E}_d^2}{4\tilde{V}^2 x} \right)^{1/3} - 1, \\ B &= \sqrt{\frac{\tilde{E}_d^2}{\tilde{V}^2 x A}} - A - 3. \end{aligned} \quad (\text{B3})$$

Using Eq. (B3) for μ_{\max} in Eq. (A1), we find $\max(\hbar\omega_{p0})$, which gives an explicit expression for the lossless plasmonic region when $\tilde{E}_d < \tilde{V}\sqrt{x}$,

$$\sqrt{\frac{8\alpha}{3\pi}} \left(\frac{2mc^2}{E_m} \right)^{1/4} \left(\frac{\tilde{V}^2 x}{\tilde{E}_d - \tilde{\mu}_{\max}} + \tilde{\mu}_{\max} \right)^{3/4} \left(\frac{(\tilde{E}_d - \tilde{\mu}_{\max})^2}{(\tilde{E}_d - \tilde{\mu}_{\max})^2 + \tilde{V}^2 x} \right)^{3/2} > \frac{\tilde{E}_d + \sqrt{\tilde{E}_d^2 + 4\tilde{V}^2 x}}{2}. \quad (\text{B4})$$

The combination of Eq. (B2) and Eq. (B4) defines the lossless region in the HMA parameter space for the case of $\ell = 0$, shown by the solid black contour in Fig. 3 of the text.

Appendix C: BAC parameters of $\text{Zn}_{1-y}\text{Cd}_y\text{Te}_{1-x}\text{O}_x$

Table I shows the BAC parameters of $\text{Zn}_{1-y}\text{Cd}_y\text{Te}_{1-x}\text{O}_x$ for $y = 0$ and $y = 1$ extracted primarily from optical measurements.^{39,40,46–48} We include bowing for E_d using $E_d(y) = (1 - y)E_d|_{y=0} + yE_d|_{y=1} + y(1 - y)C$, with $C = 0.46$ eV,^{39,49} while for V and m , we used linear interpolation between the values shown in Table I.

The two dashed green lines in Fig. 3 show the locus of ZnCdTeO for two different fractions of oxygen as y changes. The lines are not perfectly vertical, but they are nearly so because $V\sqrt{x}$ varies much less than E_d for the same range of y . Also, both V and m decrease with a similar rate as y increases, leaving $V/E_m \propto V/m$ nearly unchanged.

REFERENCES

- ¹R. H. Ritchie, “Plasma losses by fast electrons in thin films,” *Phys. Rev.* **106**, 874–881 (1957).
- ²C. J. Powell and J. B. Swan, “Effect of oxidation on the characteristic loss spectra of aluminum and magnesium,” *Phys. Rev.* **118**, 640–643 (1960).
- ³S. A. Maier *et al.*, *Plasmonics: fundamentals and applications*, Vol. 1 (Springer, 2007).
- ⁴W. L. Barnes, A. Dereux, and T. W. Ebbesen, “Surface plasmon subwavelength optics,” *Nature* **424**, 824–830 (2003).

⁵E. Ozbay, “Plasmonics: Merging photonics and electronics at nanoscale dimensions,” *Science* **311**, 189–193 (2006).

⁶A. M. Urbas, Z. Jacob, L. D. Negro, N. Engheta, A. D. Boardman, P. Egan, A. B. Khanikaev, V. Menon, M. Ferrera, N. Kinsey, C. DeVault, J. Kim, V. Shalaev, A. Boltasseva, J. Valentine, C. Pfeiffer, A. Grbic, E. Narimanov, L. Zhu, S. Fan, A. Alù, E. Poutrina, N. M. Litchinitser, M. A. Noginov, K. F. MacDonald, E. Plum, X. Liu, P. F. Nealey, C. R. Kagan, C. B. Murray, D. A. Pawlak, I. I. Smolyaninov, V. N. Smolyaninova, and D. Chanda, “Roadmap on optical metamaterials,” *J. Opt.* **18**, 093005 (2016).

⁷M. Kauranen and A. V. Zayats, “Nonlinear plasmonics,” *Nat. Photonics* **6**, 737–748 (2012).

⁸X. Guo, Y. Ma, Y. Wang, and L. Tong, "Nanowire plasmonic waveguides, circuits and devices," *Laser Photonics Rev.* **7**, 855–881 (2013).

⁹Z. Han and S. I. Bozhevolnyi, "Radiation guiding with surface plasmon polaritons," *Rep. Prog. Phys.* **76**, 016402 (2012).

¹⁰M. I. Stockman, "The spaser as a nanoscale quantum generator and ultrafast amplifier," *J. Opt.* **12**, 024004 (2010).

¹¹H. A. Atwater and A. Polman, "Plasmonics for improved photovoltaic devices," in *Materials for Sustainable Energy* (World Scientific, 2011) pp. 1–11.

¹²M. Li, S. K. Cushing, and N. Wu, "Plasmon-enhanced optical sensors: a review," *Analyst* **140**, 386–406 (2015).

¹³W. Hou and S. B. Cronin, "A review of surface plasmon resonance-enhanced photocatalysis," *Adv. Funct. Mater.* **23**, 1612–1619 (2013).

¹⁴M. Fleischmann, P. Hendra, and A. McQuillan, "Raman spectra of pyridine adsorbed at a silver electrode," *Chem. Phys. Lett.* **26**, 163–166 (1974).

¹⁵M. S. Tame, K. McEnery, S. Özdemir, J. Lee, S. A. Maier, and M. Kim, "Quantum plasmonics," *Nat. Phys.* **9**, 329–340 (2013).

¹⁶X. Jiang, P. Chen, K. Qian, Z. Chen, S. Xu, Y.-B. Xie, S. Zhu, and X. Ma, "Quantum teleportation mediated by surface plasmon polariton," *Sci. Rep.* **10**, 1–8 (2020).

¹⁷S. V. Boriskina, T. A. Cooper, L. Zeng, G. Ni, J. K. Tong, Y. Tsurimaki, Y. Huang, L. Meroueh, G. Mahan, and G. Chen, "Losses in plasmonics: from mitigating energy dissipation to embracing loss-enabled functionalities," *Adv. Opt. Photon.* **9**, 775–827 (2017).

¹⁸J. B. Khurgin and A. Boltasseva, "Reflecting upon the losses in plasmonics and metamaterials," *MRS Bull.* **37**, 768–779 (2012).

¹⁹J. B. Khurgin and G. Sun, "Scaling of losses with size and wavelength in nanoplasmonics and metamaterials," *Appl. Phys. Lett.* **99**, 211106 (2011).

²⁰J. B. Khurgin, "How to deal with the loss in plasmonics and metamaterials," *Nat. Nanotechnol.* **10**, 2–6 (2015).

²¹G. Baffou and R. Quidant, "Thermo-plasmonics: using metallic nanostructures as nano-sources of heat," *Laser Photonics Rev.* **7**, 171–187 (2013).

²²M. I. Stockman, K. Kneipp, S. I. Bozhevolnyi, S. Saha, A. Dutta, J. Ndukaife, N. Kinsey, H. Reddy, U. Guler, V. M. Shalaev, A. Boltasseva, B. Gholipour, H. N. S. Krishnamoorthy, K. F. MacDonald, C. Soci, N. I. Zheludev, V. Savinov, R. Singh, P. Groß, C. Lienau, M. Vadai, M. L. Solomon, I. Barton, David R., M. Lawrence, J. A. Dionne, S. V. Boriskina, R. Esteban, J. Aizpurua, X. Zhang, S. Yang, D. Wang, W. Wang, T. W. Odom, N. Accanto, P. M. de Roque, I. M. Hancu, L. Piatkowski, N. F. van Hulst, and M. F. Kling, "Roadmap on plasmonics," *J. Opt.* **20**, 043001 (2018).

²³Y. Wu, C. Zhang, N. M. Estakhri, Y. Zhao, J. Kim, M. Zhang, X. Liu, G. K. Pribil, A. Alù, C. Shih, and X. Li, "Intrinsic optical properties and enhanced plasmonic response of epitaxial silver," *Adv. Mater.* **26**, 6106–6110 (2014).

²⁴M. I. Stockman, "Nanoplasmonics: past, present, and glimpse into future," *Opt. Express* **19**, 22029–22106 (2011).

²⁵B. Luk'yanchuk, N. I. Zheludev, S. A. Maier, N. J. Halas, P. Nordlander, H. Giessen, and C. T. Chong, "The fano resonance in plasmonic nanostructures and metamaterials," *Nat. Mater.* **9**, 707–715 (2010).

²⁶G. V. Naik, V. M. Shalaev, and A. Boltasseva, "Alternative plasmonic materials: beyond gold and silver," *Adv. Mater.* **25**, 3264–3294 (2013).

²⁷P. West, S. Ishii, G. Naik, N. Emani, V. Shalaev, and A. Boltasseva, "Searching for better plasmonic materials," *Laser Photonics Rev.* **4**, 795–808 (2010).

²⁸G. V. Naik, J. Liu, A. V. Kildishev, V. M. Shalaev, and A. Boltasseva, "Demonstration of Al:ZnO as a plasmonic component for near-infrared metamaterials," *P. Natl. A. Sci.* **109**, 8834–8838 (2012).

²⁹G. V. Naik, J. L. Schroeder, X. Ni, A. V. Kildishev, T. D. Sands, and A. Boltasseva, "Titanium nitride as a plasmonic material for visible and near-infrared wavelengths," *Opt. Mater. Express* **2**, 478–489 (2012).

³⁰S. Law, D. C. Adams, A. M. Taylor, and D. Wasserman, "Mid-infrared designer metals," *Opt. Express* **20**, 12155–12165 (2012).

³¹P. Jung, A. V. Ustinov, and S. M. Anlage, "Progress in superconducting metamaterials," *Supercond. Sci. Technol.* **27**, 073001 (2014).

³²J. B. Khurgin and G. Sun, "In search of the elusive lossless metal," *Appl. Phys. Lett.* **96**, 181102 (2010).

³³H. Kim, "Novel plasmon resonances of nonstoichiometric alumina," *Appl. Surf. Sci.* **488**, 648–655 (2019).

³⁴M. N. Gjerding, M. Pandey, and K. S. Thygesen, "Band structure engineered layered metals for low-loss plasmonics," *Nat. Commun.* **8**, 1–8 (2017).

³⁵J. B. Khurgin, "Mitigating the loss in plasmonics and metamaterials," Tech. Rep. (Johns Hopkins University Baltimore United States, 2017).

³⁶B. Saha, A. Shakouri, and T. D. Sands, "Rocksalt nitride metal/semiconductor superlattices: A new class of artificially structured materials," *Appl. Phys. Rev.* **5**, 021101 (2018).

³⁷W. Shan, W. Walukiewicz, J. W. Ager, E. E. Haller, J. F. Geisz, D. J. Friedman, J. M. Olson, and S. R. Kurtz, "Band anticrossing in GaInAs alloys," *Phys. Rev. Lett.* **82**, 1221–1224 (1999).

³⁸H. Allami and J. J. Krich, "Plasma frequency in doped highly mismatched alloys," *Phys. Rev. B* **103**, 035201 (2021).

³⁹T. Tanaka, K. Mizoguchi, T. Terasawa, Y. Okano, K. Saito, Q. Guo, M. Nishio, K. M. Yu, and W. Walukiewicz, "Compositional dependence of optical transition energies in highly mismatched $Zn_{1-x}Cd_xTe_{1-y}O_y$ alloys," *Appl. Phys. Express* **9**, 021202 (2016).

⁴⁰S. Adachi, *Properties of group-IV, III-V and II-VI semiconductors* (John Wiley & Sons, 2005) Chap. 7, p. 150.

⁴¹T. Tanaka, K. Matsuo, K. Saito, Q. Guo, T. Tayagaki, K. M. Yu, and W. Walukiewicz, "Cl-doping effect in $ZnTe_{1-x}O_x$ highly mismatched alloys for intermediate band solar cells," *J. Appl. Phys.* **125**, 243109 (2019).

⁴²W. Walukiewicz and J. M. O. Zide, "Highly mismatched semiconductor alloys: From atoms to devices," *J. Appl. Phys.* **127**, 010401 (2020).

⁴³J. Zhang, Y. Wang, S. Khalid, A. Janotti, G. Haugstad, and J. M. O. Zide, "Strong band gap reduction in highly mismatched alloy InAlBiAs grown by molecular beam epitaxy," *J. Appl. Phys.* **126**, 095704 (2019).

⁴⁴V. Pačebutas, S. Staniotynė, R. Norkus, A. Bičiūnas, A. Urbanowicz, and A. Krotkus, "Terahertz pulse emission from GaInAsBi," *J. Appl. Phys.* **125**, 174507 (2019).

⁴⁵H. Allami, "Lossless HMAs," (2022).

⁴⁶M. Welna, R. Kudrawiec, Y. Nabetani, T. Tanaka, M. Jaquez, O. D. Dubon, K. M. Yu, and W. Walukiewicz, "Effects of a semiconductor matrix on the band anticrossing in dilute group II-VI oxides," *Semicond. Sci. Technol.* **30**, 085018 (2015).

⁴⁷K. M. Yu, W. Walukiewicz, W. Shan, J. Wu, J. W. Beeman, M. A. Scarpulla, O. D. Dubon, and P. Becla, "Synthesis and optical properties of II-O-VI highly mismatched alloys," *J. Appl. Phys.* **95**, 6232–6238 (2004).

⁴⁸M. J. Seong, I. Miotkowski, and A. K. Ramdas, "Oxygen iso-electronic impurities in znte: Photoluminescence and absorption spectroscopy," *Phys. Rev. B* **58**, 7734–7739 (1998).

⁴⁹B. Samanta, S. Sharma, and A. Chaudhuri, "Study of the microstructure and optical properties of polycrystalline $Cd_{1-x}Zn_xTe$ thin films," *Vacuum* **46**, 739–743 (1995).